X-Ray Computed Tomography Studies of Gas Storage and Transport in Devonian Shales

X. Lu, P. Miao, and A. T. Watson
Dept. of Chemical Engineering, Texas A&M University, College Station, TX 77843

G. P. Pepin and R. M. Moss
Texaco, Inc., Houston, TX 77215

M. Semmelbeck
S. A. Holditch & Associates Inc., College Station, TX 77840

Devonian shales and other unconventional resources can be highly fractured and may have significant amounts of gas stored by adsorption. Conventional experiments are not well suited for characterizing the properties important for describing gas storage and transport in these media. Here, X-ray computed tomography scanning is used to determine gas storage in dynamic gas flow experiments on Devonian shale samples. Several important properties are obtained from these experiments, including fracture widths, adsorption isotherms, and matrix porosities and permeabilities.

Introduction

Unconventional resources such as Devonian shales and coal seams have long been recognized as major sources for natural gas. It has been estimated that more than one thousand trillion standard cubic feet (Tcf) of gas are contained in Devonian shale formations in the Appalachian basin (Smith, 1978), and several hundred trillion standard cubic feet of gas are contained in the major U.S. coal reserves (Kuuskraa and Branderburg, 1989). However, the mechanisms whereby gas is stored and transported in these formations are not presently well understood. In addition to conventional storage as "free" gas in the pore space, significant amounts of gas are stored as a condensed phase due to gas adsorption on matrix surfaces and/or solution in organic material. Studies have indicated that 50% or more of the natural gas stored in Devonian shales may exist as a condensed phase (Thomas and Frost, 1989; Lane et al., 1991a). These unconventional resources are typically fractured. They have very small matrix permeabilities, and fractures are important for significant production.

Properties which are important for describing the transport and storage of gas in shales and coal are not determined well by conventional experiments. For example, the extremely small matrix permeabilities and porosities may not be reliably determined by standard techniques. Determination of such small values may typically require greater equipment resolution than is currently available or substantially greater experimental times than are feasible. Properties of fractured media are not described well with conventional experiments. Permeabilities associated with fractures or laminae separations may be orders of magnitude higher than those associated with the matrix. Conventionally measured rock properties only represent an averaged value of the sample which would depend highly on the particular fracture system of the sample. Furthermore, any induced fractures would completely invalidate the measured values. Finally, analyses of conventional experiments do not take into account the existence of condensed-phase gas storage.

X-ray computed tomography (CT) can be an important tool for study of unconventional resources and other fractured media. There have been a number of published applications of CT scanning in reservoir characterization (Withjack et al., 1991; Kantzas, 1990; Hicks et al., 1992) and fluid flow visualization (Wang et al., 1984; Peters and Hardham, 1990; Vinegar and Wellington, 1987; Hove et al., 1987). Many of these studies have only dealt with qualitative analyses of CT images and have not sought to determine properties useful for describing fluid storage or transport. Quantitative estimates of the porosity distribution for conventional samples can be determined by a dual-scan method (Withjack, 1988; Kantzas, 1990; Moss et al., 1992; Hicks et al., 1992). This involves a pixel-by-pixel subtraction of CT images determined when the sample is fully saturated with a fluid and when it is evacuated. This technique is most conveniently carried out using a gas. Moss et al. (1992) demonstrated the technique using xenon, a

radio opaque gas, with several sandstone, carbonate and shale samples. A radio opaque gas is required to achieve sufficient contrast in the images to determine the porosity accurately.

Watson and Mudra (1991) investigated the use of the dual-scan technique for characterization of Devonian shales. X-ray attenuation depends on the actual amount of the fluid phase which is present. When a condensed phase is present, the dual-scan method can be used to determine the total amount of the saturating fluid present at each voxel, rather than the porosity. The storage, which is defined as the ratio of the amount of saturating fluid per unit bulk volume of porous media to the bulk gas density (Watson and Mudra, 1991), is a useful representation for the amount of saturating fluid.

The determination of storage distributions with both krypton and xenon has been demonstrated with Devonian shales (Watson and Mudra, 1991; Lu et al., 1992). In those experiments, storage distributions were determined dynamically as gas permeated a sample that was initially evacuated. These studies clearly demonstrated the role of fractures for gas transport in the shales and provided independent evidence of the existence of a condensed phase.

In conventional resources, knowledge of the porosity distribution with an equation of state for the saturating fluid is sufficient for describing the fluid storage as a function of pressure. In the unconventional resources, the variation of the storage with pressure is a function of the porous medium, not simply described with the porosity. This storage is typically described as a sum of the amount of "free" gas present in the pore space and the amount of condensed fluid phase. In this work, data from CT scanning are used to determine the amount of the condensed phase as a function of pressure. The results are validated with adsorption isotherms obtained from independent experiments. Evidence shows that krypton, which was used as the saturation fluid, and methane have very similar adsorption properties in shales, so that krypton provides a good model for inferring the behavior of natural gas in the shales. Properties useful for describing fluid transport include permeabilities associated with fractures and matrix material. A method is described to estimate fracture widths from CT images. This information can be used to estimate fracture permeabilities and for modeling the dynamic experiments to estimate other properties. Detailed simulations of the dynamic experiments are used to infer values for matrix permeabilities and porosities.

Experiment

Gas flow

The experiments were performed on a fourth-generation Technicare 2060 CT scanner at Texaco E&P Technology Department. The scanner produces 512×512 pixel images in which each pixel represents a $0.25 \times 0.25 \times 2.0$ (mm) volume element. A 120 kev, 75 mA X-ray source was used for the experiments. The resulting CT images were analyzed on a MicroVax 3800 computer. The image analysis software was developed at Texaco using the IDL programming language.

To perform the experiments, Figure 1, cylindrical shale plugs were mounted in a thin-walled aluminum core barrel. There was no confining pressure applied on the core samples, so the saturating gas entered the sample from all directions during gas flow. The plugs were first evacuated, and CT scans were

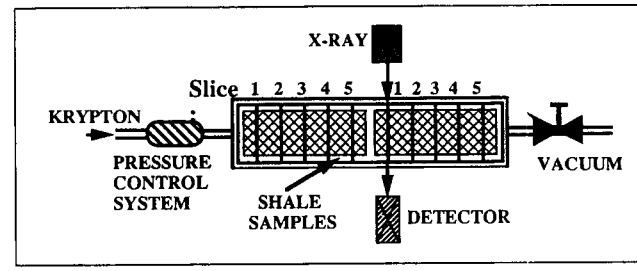

Figure 1. Experimental arrangement.

taken at selected slices (five slices were selected for each plug as shown in Figure 1). The CT images taken with the samples evacuated were used as the background images. To begin the gas flow, krypton gas was quickly introduced into the core barrel and pressure was maintained at a preset level. A series of scans were made at the same slices as for the evacuated scans while gas invasion was in progress. The interscan time varied from a few minutes at the beginning of the gas flow to several hours toward the end of the experiment. The gas storage images were obtained by subtracting the background image from the images taken during gas invasion. The gas flow experiments were performed at four pressures (1.83, 2.86, 4.24 and 6.72 MPa). All of the experiments were performed at room temperature.

Two Devonian shale samples were used in this study. They were from Gas Research Institute's Comprehensive Study Well (CSW) Program. The samples were cut as 3.81 cm dia. cylindrical plugs with bedding planes parallel to the axis. The length of each plug is 6.35 cm. Some physical parameters for companion plugs (Guidry et al., 1990) are listed in Table 1. Before the experiment, the samples were evacuated at 50–60°C for two days to remove any moisture and residual gas. Between the experiments, the shale plugs were evacuated at room temperature to remove the krypton gas. After the gas flow experiments, thin section analyses were performed on the samples.

Although the basic technique of the CT scanning experiment is fairly straightforward, a number of factors can seriously affect the measurement accuracies if the experimental conditions are not carefully controlled, such as the scanner setup (scan time, X-ray tube current, slice thickness), core holder material and thickness, and the beam hardening effect. The scanner was carefully calibrated with fused quartz crystal, a homogeneous material with a density near that of shale samples, to reduce the beam hardening effect, and various works were performed to minimize the overall measurement errors (Moss et al., 1992).

Adsorption

The adsorption isotherm measurements were performed in a volumetric adsorption apparatus built at Texas A&M Uni-

Table 1. Physical Parameters of Shale Samples Used in Experiments

Sample	Bulk Density (g/cm^3)	Grain Density (g/cm^3)	Porosity (%)	Color
CSW5-4178.5	2.72	2.77	3.0	Grey
CSW5-4153.1	2.69	2.75	3.8	Grey

versity (Lu et al., 1993). The main parts of the apparatus are the reference cell and the sample cell. The amount of adsorbed gas in the samples was obtained by monitoring the amount of gas charged into the reference cell and the remaining "free" gas left after introducing gas into the sample cell. The cell volumes were calibrated using gas expansions with a volume standard obtained from National Institute of Standard and Technology (Bowman et al., 1967). The temperature of the cells was maintained to within ± 0.005°C of the preset values.

The samples used in the adsorption measurements were crushed particles rather than whole plugs to avoid extremely long measurement times. The shale samples were crushed to 18–25 mesh size with an average particle size of 0.8 mm. The crushed samples were evacuated for 24 hours at 50–60°C to remove moisture and residual gases. The bulk densities of the samples were measured using a mercury porosimeter.

Two gas storage quantities were measured: the amount of adsorbed gas and the amount of total stored gas. The adsorbed gas includes the condensed gas on the shale matrix and pore surfaces, while the total stored gas is the sum of adsorbed gas and the "free" gas in the pore spaces.

Analysis of Experiments

Storage

X-ray CT scanning measures the localized X-ray linear attenuation coefficients, μ, within the scanned object. The measurement values are normally expressed as CT numbers, CTN, computed by the equation:

$$\text{CTN} = 1{,}000\,\frac{\mu_s - \mu_w}{\mu_w} \tag{1}$$

where μ_s is the linear attenuation coefficient for the scanned object, and μ_w is the linear attenuation coefficient for water.

To relate the CT number to the amount of saturating fluid in the porous medium, the fluid storage, S, for a voxel is defined as:

$$S = \frac{\varrho_f}{\rho_g^*} \tag{2}$$

which is the ratio of the saturating fluid mass in the voxel to the corresponding fluid mass that would occupy a voxel as a bulk fluid phase at the pressure and temperature external to the porous media. In Eq. 2, ϱ_f represents the amount of fluid per unit bulk volume of the porous media, and ρ_g^* represents the density of the bulk fluid phase. The superscript * refers to the conditions external to the porous media. The fluid storage in a porous media can be related to the linear attenuation coefficient (Watson and Mudra, 1991; Lu et al., 1992), and hence the CT number by:

$$S = \frac{\mu_f}{\mu_g^*} = \frac{\mu_s - \mu_r}{\mu_g^*} \tag{3}$$

Here, the subscripts s, r, and g correspond to porous media saturated with fluid, evacuated porous media, and gas, respectively.

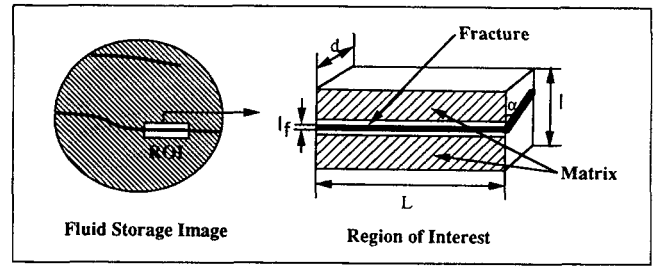

Figure 2. Region of interest used to estimate core fracture width.

Condensed-phase isotherms

It is instructive to relate the storage measured at equilibrium to the porosity when a condensed fluid phase is present in a porous medium. Assuming that the pore space is saturated by a fluid whose state can be described by the same equation of state as bulk-phase gas, the amount of fluid per unit bulk volume of porous medium is:

$$\varrho_f = \rho_g \phi + \varrho_c \tag{4}$$

where ϱ_c refers to the amount of condensed-phase fluid per unit bulk volume of porous media, ρ_g is the bulk-phase fluid density, and ϕ is the porosity of the porous media. Using Eqs. 2 and 4, the storage at the equilibrium state can be expressed as:

$$S_{\text{eq}} = \phi + \frac{\varrho_c}{\rho_g^*} \tag{5}$$

Thus, the storage will exceed the porosity if a condensed phase is present. Based on Eq. 5, the condensed-phase fluid storage can be estimated from S_{eq}, an independent measurement of porosity ϕ, and an appropriate equation of state for the saturating fluid.

Estimation of fracture width

Measurements of fracture widths are useful for estimating fracture permeabilities and porosities. A method is developed here to estimate average fracture widths from CT storage images. A region of interest (ROI) is selected which contains a segment of the fracture for which we desire an estimate of the average fracture width, as shown in Figure 2. By representing the ROI as having two distinct regions, the following mass balance equation can be written:

$$\rho_g^*[V_{\text{ROI}} S_{\text{ROI}}] = \rho_g^*[V_f S_f + V_m S_m] \tag{6}$$

Here, V_f and V_m are the fracture volume and matrix volume, respectively. Assuming that the fracture is filled with free gas, a value of unity is used for S_f. Using Eq. 6 and the fact that V_{ROI} is the sum of V_f and V_m, the following expression for the volume fraction of the fracture is obtained:

$$X \equiv \frac{V_f}{V_{\text{ROI}}} = \frac{S_{\text{ROI}} - S_m}{1 - S_m} \tag{7}$$

The total storage of the ROI and matrix is easily obtained from an image analysis. If desired, S_m can be approximated as the product of the volume of the ROI and the average matrix storage. In this way, no judgment regarding which pixels occupy the fracture or matrix regions need ever be made. By assuming that the fracture is planar, the fracture width can be calculated from:

$$l_f = lX \sin \alpha \tag{8}$$

where l is the width of the ROI, and α is the angle between the fracture plane and CT image plane.

Modeling the experiment

A parameter estimation approach was used to estimate shale matrix porosity and permeability from the experimental observations. The observed data consisted of the storage distribution measured at various times as krypton gas was allowed to permeate into the core. A mathematical model was used to simulate the experiment. Values of matrix permeability and porosity were chosen so that the simulated storage distribution matched, in a least-squares sense, the observed distribution at each measurement time.

The experimental system (core sample) was modeled as a heterogeneous continuum in which the permeability and porosity were allowed to vary with position. The mathematical model is an application of a continuity equation and Darcy's law. The condensed phase is treated as a source term, and it is assumed that the condensed phase is in instantaneous equilibrium with the free gas phase (Schettler et al., 1987). The continuity equation used in this work has the following form (Collins, 1990):

$$-\vec{\nabla} \cdot (\rho_g \vec{v}) = \frac{\partial}{\partial t} (\rho_g \phi + \varrho_c) \tag{9}$$

The velocity vector in this equation is assumed to be described by the Darcy flow equation, which has the following form:

$$\vec{v} = -\frac{k}{\mu_g} \vec{\nabla} P \tag{10}$$

The effects of gravity are neglected. Also used in the model are an equation of state and adsorption isotherm to represent the gas- and condensed-phase densities, respectively, as functions of pressure. This system is solved for pressure using the following boundary conditions:

$$\begin{aligned} P &= P_i \quad \text{for } t = 0 \text{ and } 0 \le r \le r_e \\ P &= P_{inj} \quad \text{for } t > 0 \text{ and } r = r_e \\ P &= P_{inj} \quad \text{for } t > 0 \text{ and } z = 0 \text{ and } z = z_t \end{aligned} \tag{11}$$

A finite difference method was used with an implicit forward difference for the time discretization and a central difference for the space discretization. An iterative direct substitution method which is a modification of the semiimplicit formulation presented in Aziz and Settari (1979) was used to handle the nonlinear terms (the pressure-dependent fluid properties). In our method, the nonlinear terms were allowed to change during the iteration procedure. At each step in this iterative procedure, the finite difference equations were solved by a sparse matrix inversion routine. All pressure-dependent properties were represented in the simulator in tabular form and used as piecewise linear functions. The cumulative mass balance errors are less than 0.1%.

A relatively coarse spatial grid was used to represent the core samples. The fractures were, in general, planar and parallel, so a three-dimensional Cartesian coordinate system was used. The orthogonal grid was oriented to follow the fractures to the extent possible. The width of grid blocks representing fractures was approximately equal to the observed width of the fractures, and relatively larger grid blocks were used elsewhere. The grid was modified to approximate the actual shape of the core sample. This results in some grid blocks which lie outside the dimensions of the cylindrical core and annular space occupied by gas which were not included in the simulation. The boundary conditions were applied at the boundaries of the modified grid. Typically, a 20×20 grid was used to represent the sample cross section, and five grid blocks were used along the axial direction.

The simulation was further simplified by representing the sample as having two distinct regions or zones. Properties were taken to be uniform within each of the regions. The fracture zone represents the relatively high storage and permeability regions, such as those corresponding to fractures, and the matrix zone represents the relatively low porosity and permeability regions associated with the matrix material. The condensed-phase storage capacity for the fracture region was assumed to be negligible. The condensed-phase storage for the matrix region was represented by the Langmuir isotherm:

$$\varrho_c = \frac{V_L \rho_R \rho_g^* P}{P_L + P} \tag{12}$$

The viscosity, μ_g, and density, ρ_g^*, of krypton gas phase were obtained as a function of pressure from a reference (Rabinovich et al., 1988).

Properties were estimated by determining parameter values that minimize an objective function, J, which is the sum of squared differences between the mass of gas stored in selected regions as determined from the CT images and the corresponding values calculated by the simulator. The objective function, J, is given by:

$$J = \sum_i \sum_j [M^{\text{cal}}(\vec{r}_i, t_j) - M^{\text{obs}}(\vec{r}_i, t_j)]^2 \tag{13}$$

where M^{cal} denotes the simulated data, M^{obs} denotes the experimental data, $\vec{r}_i$ denotes the ith region, and t_j is the experimental time. In this work, only a single region was used; the data represented the total mass stored within one slice at various experimental times. The parameters estimated here were the matrix porosity and permeability. The minimization was carried out with a trust-region implementation of the Levenberg-Marquardt method (Lane, 1991b) that includes inequality constraints for the parameter values.

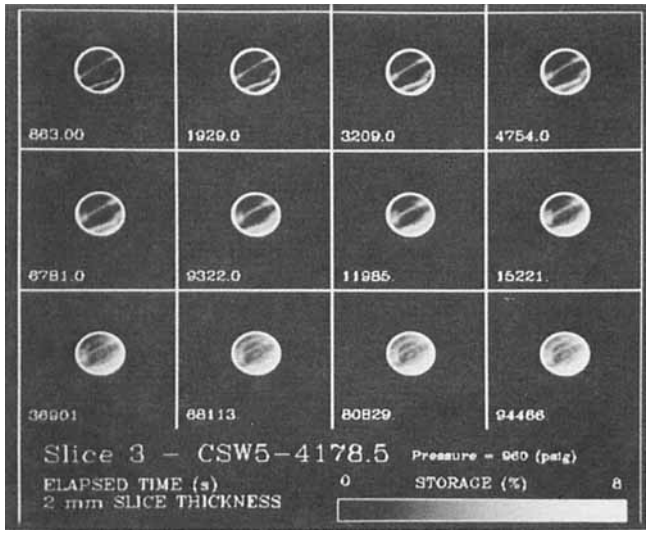

Figure 3. Gas storage images for slice 3 of sample CSW5-4178.5 with time sequence.

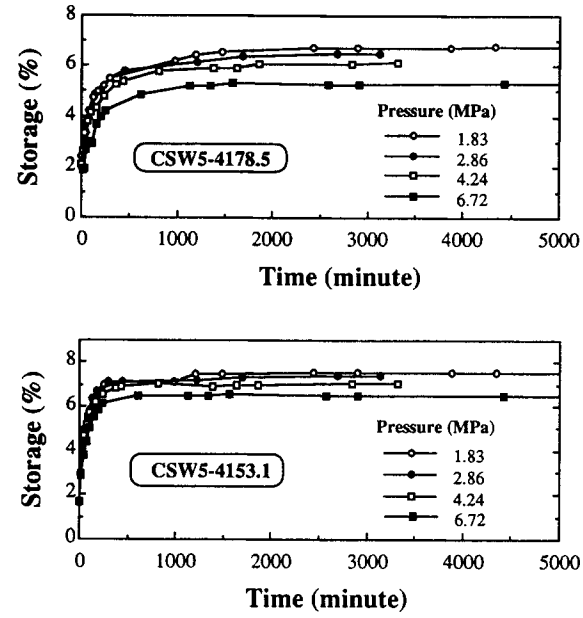

Figure 4. Averaged gas storages for various gas pressures.

Results and Discussion

Condensed-phase isotherms

Figure 3 shows a sequence of gas storage images at different gas invasion times for slice 3 of the sample CSW5-4178.5 at 6.73 MPa (960 psi) pressure. The times shown in the images are seconds after introduction of krypton gas into the core barrel. The brighter areas in the image correspond to areas with larger krypton storage. The gray scale is shown in the bottom part of the figure. From these images we see that the gas storage begins from two thin streaks, which were positively identified as fractures by subsequent thin section analysis. The widths of the bright streaks become larger with increasing time, indicating that krypton gas has penetrated the matrix areas through the fractures. These fractures act as conduits for gas transport into the Devonian shales. Little change in gas storage is observed in the last three images, for which the gas storage times exceed 20 h (72,000 s), indicating that gas storage equilibrium has been established.

Average gas storages as a function of time for various experimental pressures are shown in Figure 4 for the two samples. This average gas storage was determined as the average over the five scanned slices in each of the samples. Note that the storage decreases with increasing pressure. This is direct evidence of a condensed phase. In the absence of a condensed phase, the storage would be constant, as indicated by Eq. 5. The *decrease* in storage with increasing pressure is consistent with a description of the condensed phase as following a Langmuir-type nonlinear adsorption isotherm. The amount of condensed gas can be calculated from the equilibrium gas storage, S_{eq}, using Eq. 5. The total amount of stored gas and the amount of the condensed phase, expressed in units of std. m^3/m^3, are listed in Table 2. The fraction of the fluid that is stored as a condensed phase, also in Table 2, ranges from 40–60%. During these calculations, the average porosities in Table 1 and the average equilibrium storage corresponding to the entire sample are used. Therefore, the storage value so calculated is the average value corresponding to the entire sample. The total storage and amount of the condensed phase are compared with those obtained from the adsorption experiment in Figure 5. The condensed-phase gas storages measured by the two different experiments are consistent. The larger values of total gas storage measured by the adsorption method are to be expected since crushed samples were used during the adsorption measurement. A recent study showed that crushing Devonian shale samples may result in larger porosity values when compared to those obtained from whole shale plugs (Luffel and Guidry, 1992). The larger porosity for crushed samples is the reason for larger total gas storage observed in the adsorption experiment.

To investigate whether adsorption of krypton is representative of the behavior of natural gas, krypton and methane adsorption isotherms were measured. Figure 6 shows the adsorption isotherms of krypton and methane measured on two samples. The isotherms, both total stored and adsorbed, for the two gases are very close; the differences are less than 16%. This indicates that the gas storage of methane and krypton

Table 2. Equilibrium Gas Storage and Condensed Gas Amounts for Samples CSW5-4178.5 and CSW5-4153.1

	CSW5-4178.5				CSW5-4153.1			
Pressure (MPa)	1.83	2.86	4.24	6.72	1.83	2.86	4.24	6.72
Storage (%)	6.75	6.46	6.12	5.34	7.52	7.40	7.02	6.54
Total gas stored (std. m^3/m^3)	1.07	1.63	2.32	3.24	1.19	1.87	2.66	3.97
Condensed phase (std. m^3/m^3)	0.592	0.875	1.19	1.42	0.591	0.915	1.23	1.67
Fraction condensed (%)	55.3	53.6	51.3	43.8	49.7	48.9	46.2	42.1

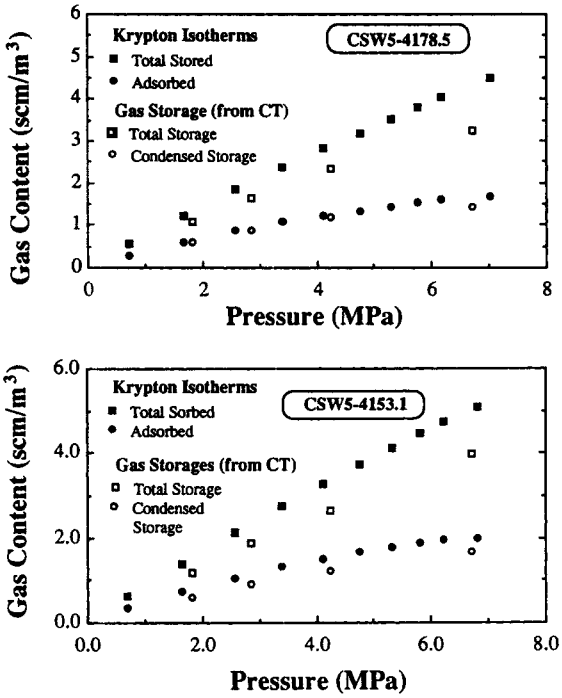

Figure 5. Comparison of gas storage obtained from adsorption experiment and CT scan experiment.

gases on Devonian shale are very similar and that krypton gas is a reasonable model for studying natural gas storage in Devonian shales.

Estimation of fracture width

Figure 7 shows examples of regions of interest (ROI) and

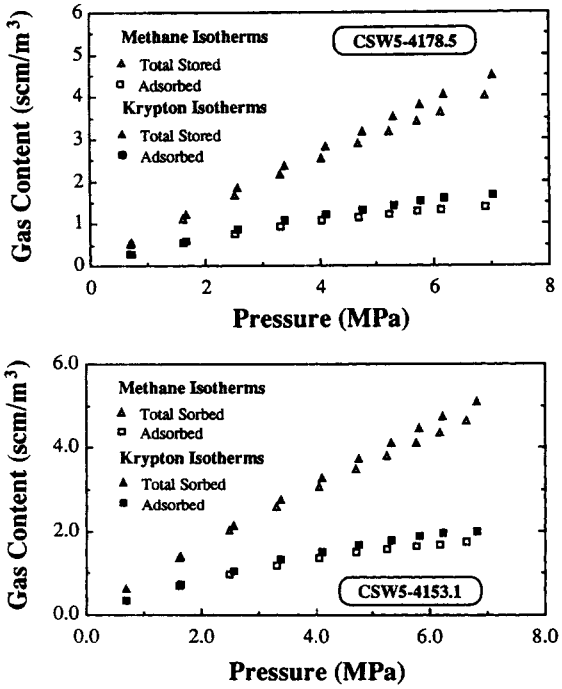

Figure 6. Adsorption isotherms of methane and krypton on two CSW5 samples.

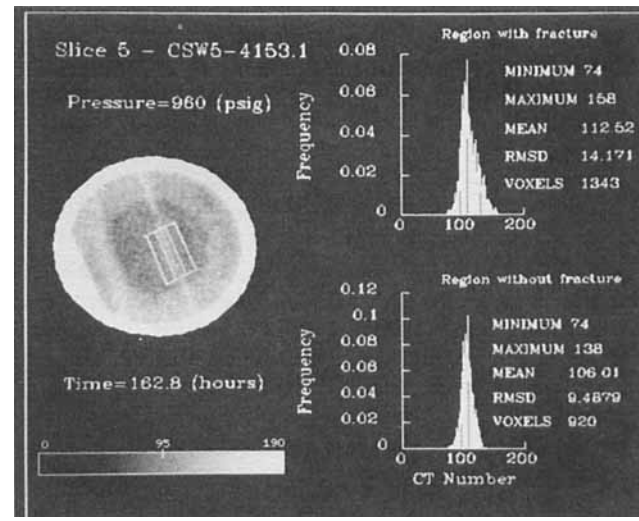

Figure 7. Example of region of interest used to estimate core fracture width.

statistics of gas storage images used for estimating fracture width. The gas storage distribution of this sample is relatively homogeneous; the darker area at the center of the image is caused by the beam hardening effect. Two fractures are visible in this image which correspond to the two brighter streaks. The estimate was obtained for the fracture located at the center of the image. An estimate of the fracture width from a photograph of a thin section prepared subsequently was 10 micron. Our estimates were performed under different scenarios: 1) for various degrees of gas saturation (the degree of gas saturation is defined as the ratio of gas storage to the equilibrium gas storage); 2) for two different ROIs. The results are listed in Table 3. The fracture width estimated from two different ROIs are in agreement, which indicates that this method is independent of the selection of ROI when there is a relatively homogeneous gas storage distribution in the matrix. The estimated fracture width decreases with increasing gas saturations and eventually reaches a constant (within a certain error range) when the equilibrium gas saturation is reached. The reason is that the region used to calculate the matrix gas storage S_m does not include matrix areas adjacent to the fracture (Fig-

Table 3. Fracture Width Estimations for Slice 5 Plug CSW5-4153.1 at Pressure of 6.72 MPa*

Deg of Sat. (%)	ROI 1 (l=25.5 Pixel) X (%)	ROI 1 l_f (μm)	ROI 2 (l=20.1 Pixel) X (%)	ROI 2 l_f (μm)
82	0.654	41.6	-	-
87	0.539	34.4	-	-
92	0.470	30.0	0.539	27.1
97	0.380	24.2	-	-
98	0.357	22.8	-	-
98	0.348	22.2	-	-
99	0.347	22.1	0.438	22.0
100	0.331	21.1	-	-
100	0.316	20.1	-	-
100	0.293	18.7	0.374	18.8
100	0.317	20.2	-	-
100	0.300	19.1	-	-
100	0.288	18.4	0.397	19.9

*Estimated from thin section analysis: 10 (μm).

Table 4. Estimates of Matrix Porosities and Permeabilities at Various Pressures

	Shale Parameters							
	1.83 MPa		2.86 MPa		4.24 MPa		672 MPa	
Sample	k_m (nd)	ϕ_m (%)	k_m (nd)	ϕ_m (%)	k_m (nd)	ϕ_m (%)	k_m (nd)	ϕ_m (%)
CSW5-4153.1	5.62	3.93	4.24	3.60	2.34	3.79	1.07	3.95
CSW5-4178.5	3.65	2.75	2.16	2.73	2.07	2.85	0.61	2.55

ures 2 and 7). Early in the gas invasion, the gas storage in the matrix areas adjacent to the fracture is larger than the rest of the matrix areas. Hence, the matrix gas storage S_m is underestimated at early gas saturation times, and according to Eqs. 7 and 8, the fracture width is overestimated. Therefore, it is recommended that the estimates be made at equilibrium gas storage conditions. The fracture width estimated by CT image analysis is larger than that estimated by thin section analysis. One reason may be that we assumed the angle between fracture plane and CT image plane, α, is 90°. This assumption results in the maximum possible width for the fracture according to Eq. 8. But it is also possible that the fracture width of the prepared thin section may differ from the fracture width of the sample as used in the CT scan experiment.

Estimation of matrix properties

For each sample, the total storage for the third slice at various times was used to estimate the matrix permeability and porosity through minimization of the objective function given by Eq. 13. Since the relative contributions of gas storage from fractures to the total gas storage of the entire slice are very small, the properties associated with the fractures could not be accurately estimated from this representation of the data. The fracture permeabilities were calculated based on a simplified model (Parsons, 1966) using the widths estimated by image analysis. The simulated results were fairly insensitive to fracture porosity because of the relatively small amount of fluid contained in that region. Langmuir isotherms fitted to the gas storages (Lane et al., 1991a) in Table 2 were used to represent the condensed-phase isotherms.

The parameter estimation results for two samples at various gas pressures are listed in Table 4, and the comparisons of experimental data and simulated data for the two samples are shown in Figure 8. The simulated data match the experimental data fairly well. Table 4 shows that the permeabilities depend strongly on the gas pressures, decreasing with increasing gas pressure. There may be two reasons for this phenomenon. One is the Klinkenberg effect (Collins, 1990; Jacob, 1972). According to fluid mechanics, whenever the mean free path of the gas molecules approaches the dimensions of the flow conduit, the individual gas molecules are in collision with the surface of conduit as well as with other gas molecules. This will contribute an additional flux, hence an observed increase in gas permeability. Over the pressure range of 1.83 to 6.73 MPa at room temperature, the mean free path of krypton molecules is about 2.0–0.5 nm. The majority of the pores of the Devonian shales are believed to be less than 10 nm (Schettler and Parmely, 1991).Therefore, the mean free path of the gas molecules and the pore dimensions are comparable, and the Klinkenberg effect is likely to occur. The other reason is related to the gas adsorption. As the number of adsorbed gas molecules increases, these molecules could block or partially block some of the very small pores and increase the resistance to the gas flow. The phenomenon of decreasing gas permeability with increasing gas adsorption has been observed in coal samples (Harpalani and Zhao, 1989).

Conclusions

X-ray-computed tomography was used to characterize properties associated with the storage and transport of fluid in unconventional natural gas reservoirs. Methods were developed to estimate fracture widths and adsorption isotherms. A parameter estimation approach based on simulation of the dynamic experiments was used to estimate matrix porosities and permeabilities. These methods were demonstrated with data obtained from experiments with Devonian shales samples.

Acknowledgment

Financial support of this work by the Gas Research Institute is gratefully acknowledged. The authors would like to thank Mr. Patrick Lowry for performing petrophysical analyses and Mr. John Coats for performing CT scanning experiments.

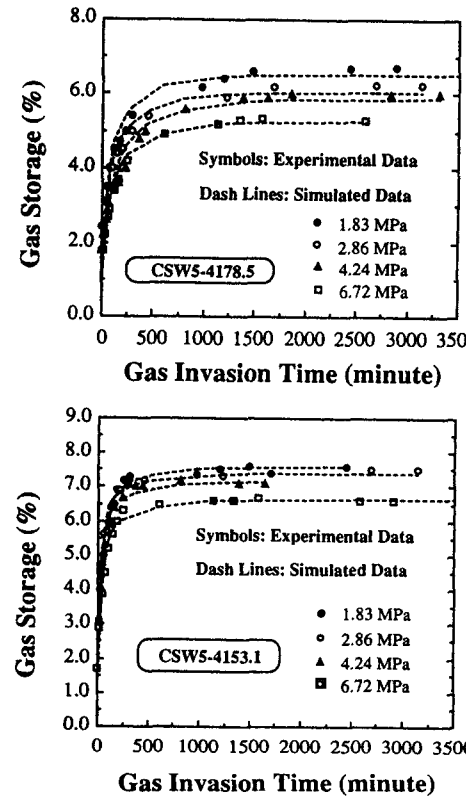

Figure 8. Comparison of experimental data and simulated data at various pressures.

Notation

CTN = CT number
k = permeability (md)
l = width of ROI (μm)
M^{cal} = simulated data
M^{obs} = experimental data
P = gas pressure (MPa)
P_i = initial pressure (MPa)
P_{inj} = injected gas pressure (MPa)
P_L = Langmuir pressure parameter (MPa)
r = radius (cm)
r_e = core sample radius (cm)
$\vec{r}_i$ = ith region of grid block
ROI = region of interest
S = fluid storage (%)
t = gas invasion time (s)
$\vec{t}_j$ = jth experimental time (s)
$\vec{v}$ = superficial gas velocity (cm/s)
V = volume (cm^3)
V_L = Langmuir volume parameter (cm^3/g)
X = volume fraction (%)
z = cylinder length position (cm)
z_i = core sample length (cm)

Greek letters

α = angle between fracture and image planes (deg)
ϕ = porosity (%)
ρ = fluid density (g/cm^3)
ρ_g = bulk gas density (g/cm^3)
ρ_g^* = bulk gas density at conditions external to core sample (g/cm^3)
ρ_R = core sample density (g/cm^3)
ϱ = amount of fluid per unit bulk volume of porous media (g/cm^3)
ϱ_c = amount of condensed fluid per unit bulk volume of porous media (g/cm^3)
μ = X-ray linear attenuation coefficient (1/m)
μ_g = gas viscosity (Pa·s)

Superscripts and subscripts

* = conditions external to core sample
c = condensed phase
cal = simulated data
eq = equilibrium state
f = saturating fluid
g = gas phase
m = matrix
obs = experimental data
r = porous media
s = porous media saturated with fluids
w = water

Literature Cited

Aziz, K., and A. Settari, *Petroleum Reservoir Simulation*, Applied Science Publishers, London (1979).

Bowman, H. A., R. M. Schoonover, and M. W. Jones, "Procedure for High Precision Density Determinations by Hydrostatic Weighing," *J. of Res. of the Nat. Bur. of Stand.—C. Eng. and Instrum.*, 71c, No. 3 (Aug., 1967).

Collins, R. E., *Flow of Fluids Through Porous Materials*, Research & Engineering Consultants, Englewood, CO (1990).

Guidry, F. K., D. L. Luffel, A. J. Olszewski, and L. L. Raymer, *Formation Evaluation Technology for Production Enhancement*, Restech Inc., Houston Annual Technical Report to Gas Research Institute, GRI-90/0300 (Oct., 1990).

Harpalani, S., and X. Zhao, "An Investigation of the Effect of Gas Desorption on Coal Permeability," *Proc. Coalbed Methane Symposium*, Univ. of Alabama, Tuscaloosa (Apr., 1989).

Hicks, P. J., Jr., H. A. Deans, and K. Narayanan, "Distribution of Residual Oil in Heterogeneous Carbonate Cores Using X-Ray Computerized CT," *SPE Form. Eval.*, 235 (Sept., 1992).

Hove, A. O., J. K. Ringen, and P. A. Read, "Visualization of Laboratory Corefloods with the Aid of Computerized Tomography of X-Rays," *SPE Reser. Eng.*, 148-154 (May, 1987).

Jacob, B., *Dynamics of Fluid in Porous Media*, Dover Publications, New York (1972).

Kantzas, A., "Investigation of Physical Properties of Porous Rocks and Fluid Flow Phenomena in Porous Media Using Computer Assisted Tomography," *In Situ*, **14**(1), 77 (1990).

Kuuskraa, V. A., and C. F. Brandenburg, "Gas Production Report," *Oil & Gas J.*, 3 (Oct., 1989).

Lane, H. S., D. E. Lancaster, and A. T. Watson, "Characterizing the Role of Desorption in Gas Production from Devonian Shales," *Energy Res.*, **13**, 337 (1991a).

Lane, H. S., "Detection and Estimation of Gas Desorption from Devonian Shale Production and Well-Test Pressure Data," PhD Diss., Texas A & M Univ. (1991b).

Lu, X., G. P. Pepin, R. M. Moss, and A. T. Watson, "Determination of Gas Storage in Devonian Shales with X-Ray Computed Tomography," paper SPE 24810, Technical Conf. and Exhibition of SPE, Washington, DC (Oct., 1992).

Lu, X., F. Li, and A. T. Watson, "Adsorption Measurements in Devonian Shales," paper SCA 9302, Technical Conf. of Soc. of Core Analysts, Houston (Aug., 1993).

Luffel, D. L., and F. K. Guidry, "New Core Analysis Methods for Measuring Reservoir Rock Properties of Devonian Shales," *J. Pet. Tech.*, 1184 (Nov., 1992).

Moss, R. M., G. P. Pepin, and L. A. Davis, "Direct Measurement of the Constituent Porosities in a Dual Porosity Matrix," *The Log Analyst*, 126 (Mar.-Apr., 1992).

Parsons, R. W., "Permeability of Idealized Fracture Rocks," *Soc. Petrol. Eng. J.*, 126 (1966).

Peters, E. J., and W. D. Hardham, "Visualization of Fluid Displacements in Porous Media Using Computed Tomography Imaging," *SPE J.*, **4**, 155 (1990).

Rabinovich, V. A., A. A. Vasserman, V. I. Nedostup, and L. S. Veksler, *Thermophysical Properties of Neon, Argon, Krypton and Xenon*, Hemisphere, Washington, DC, p. 113 (1988).

Schettler, P. D., and C. R. Parmely, "Physical Properties of the Methane Storage and Transport in Devonian Shale," Technical Report to the Gas Research Institute, GRI Contract No. 5085-213-1143 (May, 1991).

Schettler, P. D., C. R. Parmely, and W. J. Lee, "Gas Storage and Transport in the Devonian Shales," paper 17070, SPE Eastern Regional Meeting, Pittsburgh (Oct. 21-23, 1987).

Smith, E. C., "A Practical Approach to Evaluating Shale Hydrocarbon Potential," *Eastern Gas Shale Symp. Preprints*, USDOE/METC/SP-78/6, Vol. II, p. 73 (1978).

Thomas, J., Jr., and R. R. Frost, "Adsorption/Desorption Studies of Gases through Shales," *Geological and Geochemical Studies of the New Albany Shale Group (Devonian-Mississippian) in Illinois*, R. E. Bergstrom and N. F. Shimp, eds., DOE/METC/12142-0026, p. 142 (1980).

Vinegar, H. J., and S. L. Wellington, "Tomographic Imaging of Three-Phase Flow Experiments," *Rev. Sci. Instrum.*, **58**(1), 96 (1987).

Wang, S. Y., S. Ayral, and C. C. Gryte, "Computer-Assisted Tomography for the Observation of Oil Displacement in Porous Media," *SPE J.*, **24**, 52 (1984).

Watson, A. T., and J. Mudra, "Characterization of Devonian Shales with X-Ray Computed Tomography," paper SPE 24810, *Technical Conf.* and *Exhibition of the SPE*, Dallas (Oct., 1991).

Withjack, E. M., "Computed Tomography for Rock-Property Determination and Fluid-Flow Visualization," *SPE Formation Evaluation* (Dec., 1988).

Withjack, E. M., S. K. Graham, and C.-T. Yang, "CT Determination of Heterogeneities and Miscible Displacement Characteristics," *SPE Formation Evaluation* (Dec., 1991).

Manuscript received May 12, 1993, and revision received Nov. 9, 1993.